International Journal of Adhesion & Adhesives 150 (2026) 104399

Contents lists available at ScienceDirect

International Journal of Adhesion and Adhesives

journal homepage: www.elsevier.com/locate/ijadhadh

Adhesion enhancement of PEI–PVDF interfaces in multifunctional bondlines with surface toughening based disbond arrest feature for robust and sensed composite joints

Riem Kilian [a,*], Ann-Kathrin Klein [b], Julian Steinmetz [a], Martin Johannes Schollerer [c], Christian Hühne [a,c], Andreas Dietzel [b], Oliver Völkerink [a]

[a] Institute of Mechanics and Adaptronics, Technische Universität Braunschweig, Langer Kamp 6, Braunschweig, 38106, Germany
[b] Institute of Microtechnology, Technische Universität Braunschweig, Alte Salzdahlumer Str. 203, Braunschweig, 38124, Germany
[c] Institute of Lightweight Systems, German Aerospace Center (DLR), Lilienthalplatz 7, Braunschweig, 38108, Germany

ARTICLE INFO

Dataset link: https://doi.org/10.5281/zenodo.15781418

Keywords:
Multifunctional bondline
Adhesion
Polyetherimide sensor inlay
Poly(vinylidene fluoride) surface toughening
Stick–slip behavior
Instable crack growth

ABSTRACT

Structural adhesive bonds are a desirable joining method for lightweight composite structures, but they are currently not certifiable as the sole joining method for primary joints in aircraft structures. The multifunctional bondline approach, which includes a disbond arrest technology and strain monitoring, aims to solve this problem. The multifunctional bondline consists of, in addition to the adhesive bondline, a thin film Polyetherimide (PEI) based sensor and a Poly(vinylidene fluoride) (PVDF) layer toughening the fiber reinforced plastic surface. Previous studies have shown that adhesive failures in the PEI–PVDF interface impair the functionality of the toughening layer.

This study, therefore, analyzes methods to increase the interfacial adhesion between PEI and PVDF to eliminate this weak point of the multifunctional bondline. Using physical vacuum ultraviolet (VUV), Corona, and mechanical Peel Ply methods, the adhesion enhancement is analyzed using Double Cantilever Beam and End Notched Flexure tests to determine critical energy release rate (cERR) under Mode I and II. Under Mode II, for Corona and VUV pretreatments, only the standard deviation of cERR could be reduced. However, under Mode I, the cERR value could be increased by 80 % with VUV pretreatment. Results of Energy Dispersive X-ray Spectroscopy (EDX) analysis suggest that the crack path is transferred from the PEI–PVDF interface to the PVDF film because fluoride elements were detected on the specimen half covered with PEI. This shows that the adhesive failure observed in previous studies was caused by a weak PEI–PVDF interface resulting from insufficient surface pretreatment. Peel Ply structured PEI surface decreases interfacial adhesion under Modes I and II. The significantly improved interfacial strength resulting from VUV pretreatment can pave the way for a robust multifunctional bondline. Avoiding the PEI–PVDF interface from being the weakest link in the structural bond enables the PVDF disbond-arrest function and the PEI sensor function to be retained, allowing the full potential of the base materials to be utilized.

1. Introduction

In fiber-reinforced plastics, bonded joints provide a higher lightweight potential due to the high strength-to-weight ratio compared to conventional mechanical joining techniques such as bolts or rivets. Thus, structural bonding is a key technology for lighter aicrafts with an overall increased efficiency. It should be noted that there is no universal definition for structural bonding. According to Hart-Smith [1], structural bonds transfer load between components through epoxy, phenolic, or acrylic adhesives, whereas Habenicht [2] defines structural bonding as a constructive design made possible by adhesive bonding, characterized by high strength and stiffness.

However, structural bonds alone are not yet used as primary joints in aircraft structures. Primary joints are highly load-bearing structures with a single load path. Failure of these components leads to a catastrophic loss of aircraft. Secondary joints are used in multiple load path structures. In this case, a failure of a single joint leads to a load redistribution, and thus to a minor failure consequence. Adhesive bonding in primary structures offers the greatest theoretical potential for weight savings [3]. In addition to the fact that structural bonds

* Corresponding author.
E-mail address: riem.kilian@tu-braunschweig.de (R. Kilian).

https://doi.org/10.1016/j.ijadhadh.2026.104399
Received 3 July 2025; Received in revised form 18 May 2026; Accepted 23 June 2026
Available online 30 June 2026

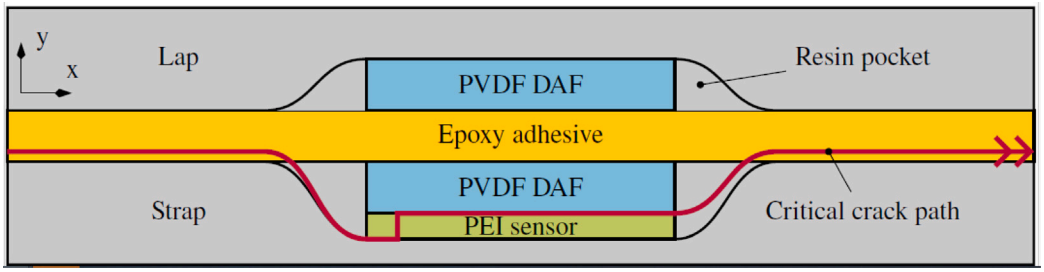

Fig. 1. Crack path in CLS specimen after crack growth indicating adhesive failure between PEI and PVDF [10].

suppress the spread of damage, a major challenge is the concern about long-term durability [4].

Therefore, a damage-tolerant design for primary bonds is needed. To ensure safety, the European Union Aviation Safety Agency and the U.S. Federal Aviation Administration state three methods for any bonded primary joint to comply with the certification specification: a maximum allowable disbond length must be determined by analysis or tests, or both and prevented by design features; proof testing must be conducted on each primary bonded production article; a reliable and repeatable non-destructive testing (NDT) method must be established [5,6]. The second method is not affordable in large commercial aircraft production, and there is no method available to measure the adhesion of the bonded joints. However, currently no NDT inspection technique able to reliably detect weak bonds is available [7]. The first method remains to be considered for practice, which leads to the need for disbond arrest methods.

The state of the art for the current certification strategy used by the aircraft industry is based on the limitation of disbond length to a maximum allowable one, through additional mechanical fasteners. Sachse et al. [8] showed that the fasteners in adhesively bonded crack lap shear specimens are effective in arresting crack growth. The observations of Chowdhury et al. [9] can support this, who proved crack arrest under static and dynamic load with additional mechanical fasteners in bonded carbon fiber reinforced plastics (CFRP) joints.

These hybrid joining methods show drawbacks in weight efficiency, reduce the adhesively bonded area, and interrupt the load path by cutting the load-bearing fibers, leading to an increased notch effect.

Surface Toughening, a more recent approach, is an advantageous method in terms of material-appropriate implementation and integration into the fiber-reinforced plastic manufacturing process. This technology involves the local application of thermoplastic films co-cured to the composite. This film shows lower stiffness and higher ductility than the adhesive and adherends. Steinmetz [10] showed the capability of Poly(vinylidene fluoride) (PVDF) as Surface Toughener in CFRP structural bonds for disbond arrest. In addition, Schollerer [11] proved with the same technology but different positioning of PVDF an increase in strength of 84 % [12] under static loads. However, the effects that lead to disbond arrest and strength increase are not yet fully understood. Damage analyses based on the method described in [13] show that these advantages are not solely attributable to the difference in stiffness and high ductility.

Heide [14] and Steinmetz [10] proposed a multifunctional bondline, which adds health monitoring functionalities to the disbond arrest feature, to overcome safety concerns without impairing the lightweight potential of the structural bonding. One key aspect studied by [10] is the functional compliance of the multifunctional bondline. This means the multifunctional bondline must bear the design loads during operation, be manufacturable using the standard thermoset CFRP curing process, and should not be heavier than state-of-the-art joining technologies. The proposed multifunctional disbond arrest feature (MDAF) consists of a smart inlay, i.e. a thin-film sensor with Polyetherimide (PEI) film as a substrate and a PVDF film as an encapsulation [15]. The smart inlay was fabricated from thin gold measuring grids, supported by a PEI layer to monitor mechanical strain at two successive fronts inside the bondline. Configured in a half-bridge structure, the system identified cracks by detecting strain gradients caused by the crack propagation.

The multimaterial layout with a PEI–PVDF interface was required because smart inlays relying solely on PEI or PVDF did not provide the sensor carrier and disbond arrest functions. PEI did not act as a Disbond Arrest Feature (DAF) [10]. Smart inlays with a PVDF substrate and a PVDF cover could not be manufactured in standard curing processes because the PVDF melted, resulting in a destroyed sensor structure [10]. PVDF-based smart inlays without an additional PVDF cover could be manufactured and acted as a DAF, but the sensor broke well before significant damage in the adhesive itself occurred. Hence, only smart inlays made of a PEI substrate with a PVDF encapsulation showed a disbond arrest function and measured the event of damage reaching the MDAF. However, the MDAF failed after the crack reached its position [10].

This was shown in cyclic crack growth tests using Cracked Lap Shear (CLS) specimens to simulate crack growth under sinusoidal tensile-tensile loading over 10^6 cycles. The CLS specimen is a doubler adhesive joint with a single free overlap edge and an artificial disbond at the overlap edge. This test method allows for crack growth experiments under realistic fatigue loads to evaluate the functional compliance of the MDAF [10].

These CLS tests showed a crack growth in the PEI-sensor-PVDF interface as depicted in Fig. 1. An additional observation was that the crack is initiated in the PEI–CFRP interface but propagates in the PEI–PVDF interface.

This weak PEI–PVDF interface mitigates the disbond arrest function of the PVDF, leading to an adhesive failure in the CLS specimens after 10^6 cycles at ultimate load (corresponding to a strain of 4000 $\mu m\ m^{-1}$ laminate strain, which is generally regarded as the ultimate operating load occurring in aerospace CFRP laminates [16]). This raises the question of how the interfacial adhesion between the two films can be increased to shift the crack path as desired to the adhesive bondline. The high interfacial adhesion between epoxy-based CFRP and PEI film is attributed to diffusion during the curing process, creating a tough interphase on a micrometer scale [17–20]. This well-studied interphase enhances the critical energy release rate (cERR) of the CFRP without affecting the strength [21,22].

The adhesion between PVDF and epoxy resin of co-cured CFRP is also based on diffusion processes forming a similar interphase but on a nanometer scale [23]. Schollerer [11] reported that additional vacuum ultraviolet (VUV) light surface pretreatment improves the adhesion in co-cured PVDF/CFRP interfaces. VUV pretreatment for PEI has also been studied in [24] in combination with the CFRP material used in [10,11]. An increase in the surface free energy but no significant increase in the interfacial strength was detected. However, the standard deviation was reduced significantly. These observations suggest that the PEI–PVDF interface adhesion could be improved through surface pretreatment. Hence, the objective of this work is to evaluate different surface pretreatment methods to increase the interfacial strength between PEI and PVDF films to move the crack path toward the

Table 1
Summary of all investigated interfaces (see Section 2.3 for the detailed layups).

Tested interface	Surface pretreatment
PEI–PVDF	–
PEI–PVDF	Corona
PEI–PVDF	VUV
PEI–PVDF	Peel Ply
PEI–CFRP	–
PVDF–CFRP	–
CFRP–CFRP	–
Adhesive-CFRP (results from [28])	Plasma

adhesive bondline or to the CFRP. The adhesion of this particular interface remains largely unexplored in the literature. For this purpose, experimental tests were carried out.

The bondline in the CLS specimen is stressed with a mixture of peel and shear loads. The mixed mode ratio between Mode I and Mode II ($MMR = G_{II}/(G_I + G_{II})$) for an equal thickness of strap and lap amounts to 0.79 [25]. Hence, the share G_{II} amounts to 0.79 and the share of G_I amounts to 0.21 [26]. Johnsen [25] and Wang [27] showed that the ratio between peel and shear within the adhesive layer remains nearly constant for varying crack lengths. It can be concluded that the CLS configuration is dominated by shear stress (Mode II) as the proportion of peel stress (Mode I) is far below the proportion of Mode II.

In order to increase the understanding of the influence of the different interfaces in the MDAF on the failure behavior, Mode I and Mode II are investigated separately.

For that matter, Double Cantilever Beam (DCB) and End Notched Flexure (ENF) tests are used to determine energy release rates of the PEI–PVDF interface with different surface pretreatment methods under Mode I and II. This quantifies the influence of the surface pretreatment on Mode I and II cERR and therefore on the mechanical properties of the multifunctional bondline. In addition, after testing the fracture surfaces are characterized by Scanning Electrone Microscopy (SEM) with energy dispersive X-ray spectroscopy (EDX) to detect the crack path based on the chemical composition of the fracture surface.

2. Material and methods

The core investigation method is to evaluate the strength of PEI–PVDF interfaces subjected to different surface pretreatments using cERR under Modes I and II. In addition, the cERR values for PEI, PVDF, and the Hysol EA9695 film adhesive from Henkel at interfaces with CFRP, as well as monolithic CFRP, are included. This enables quantifying the strength of the PEI–PVDF interfaces relative to all other interfaces present in the MDAF. Table 1 summarizes all tested interfaces, including the surface pretreatment method. The adhesive-CFRP interface has been investigated by Völkernik [28] before. Hence, his results are used for the comparison instead of repeating the experiment.

2.1. Material selection

The substrates of all specimens in this study were made from Hexcel HexPly 8552 prepreg with unidirectional IM7 carbon fibers with a nominal cured ply thickness of 0.125 mm. The amine-curing epoxy-resin system was cured according to the autoclave cycle given in the datasheet [29]. The prepreg material was combined with two thermoplastic film materials to form the interfaces under investigation. Two different Ultem 1000 PEI films with a thickness of 25 and 125 µm were used. In addition, the PVDF layer in the specimens were made from a 100 µm thin Nowoflon PVDF film.

In this study, the adherend materials (CFRP substrate) were kept constant across all specimen configurations to isolate the effect of surface pretreatment on the PEI–PVDF interfacial adhesion. Therefore, the influence of the adherend stiffness and surface energy on the measured cERR is considered constant and is not varied in this investigation.

2.2. Surface pretreatments

Numerous surface pretreatments can be applied, divided into mechanical, chemical, and physical. Widespread surface pretreatment methods for adhesive bonding are atmospheric-pressure plasma, referred to as plasma in the following, grinding, or laser pretreatments, which several authors have investigated. Mechanical pretreatments often lead to a moderate increase in bonding strength and a higher standard deviation [28,30]. Plasma, Corona, or UV-zone pretreatments are commonly used to achieve high bonding strength, resulting in cohesive failure [28,31]. Since PEI and PVDF already show high specific adhesion in the thermoset CFRP/thermoplastic film interface [22,32], only the contacting surfaces of the films are pretreated. For this purpose, Corona, Vacuum Ultraviolet Light (VUV), and Peel Ply pretreatments were performed.

Peel Ply is a removable two-dimensional micro-structured fabric layer containing polyimide that can be used for the surface of composite materials to create a reproducible surface microstructure, enabling simple demoulding. The torn fabric structure of the Peel Ply enhances the surface roughness and surface wettability of the substrate. In this case, the PEI surface is chosen to be thermally prepared with Peel Ply. The PEI represents the sensor carrier and encapsulation layer. Encapsulation was performed using a diffusion-welding process at 230°C (T_m = 250°C) using a polyamide based Peel Ply (T0098, WELA). The detailed description of the applied diffusion bonding process can be found in [33]. The main reason why only PEI was chosen to be structured with Peel Ply is the fact, that the PVDF reaches its melting temperature (T_m = 165°C) during the autoclave process for laminate manufacturing (Section 2.3). Therefore, PVDF can wet the PEI during the autoclave process. This allows the PVDF to attach itself to the Peel Ply-structured PEI for an increase in mechanical adhesion.

The second method chosen is Corona pretreatment, which removes contamination and changes the surface energy of the substrate by introducing polar groups into the surface of the substrate due to Corona or electrical local discharge. Corona pretreatment was performed using a discharge system, LabTEX-X from Tantec. The system consists of a power supply, a high voltage generator, a high frequency generator (typically 100 W, 28 kV, and 50/60 kHz), a control box, and a Corona station. The Corona discharge generates a plasma that produces reactive groups like ozone, leading to oxidative modification of the substrate surface and the introduction of polar functional groups like hydroxyl, carbonyl, or carboxyl groups. This causes an increase in specific adhesion. After being cleaned, the PEI and PVDF films were placed on an HDPE plate and the discharge process was manually driven two times by a wire electrode. The distance between the electrode and substrate was 4 mm. The PEI and PVDF films were pretreated according to the recommendations of the corona discharge system with 100 W and 28 kV.

The third method performed was Vacuum Ultraviolet (VUV) radiation pretreatment using a Xenon excimer lamp that emits photons at a wavelength of 172 nm. VUV pretreatment relies on photochemical splitting of molecular bonds of polymers, which enhances the surface polarity. Arikane et al. [32] already reported the effect of VUV on PEEK films for adhesion enhancement to CFRP and proposed certain pretreatment parameters. Based on this, Schollerer [11] successfully transferred the findings to PVDF for application in CFRP, which was also used for PVDF and PEI in the present work. In this study, the pretreatment radiation energy was set to 540 mJ/cm^2 with a distance of 0.5 mm between an ExciJet 55–130 lamp and the substrate surface. The surface temperature during the VUV and Corona pretreatment did not exceed the glass temperature of the polymer.

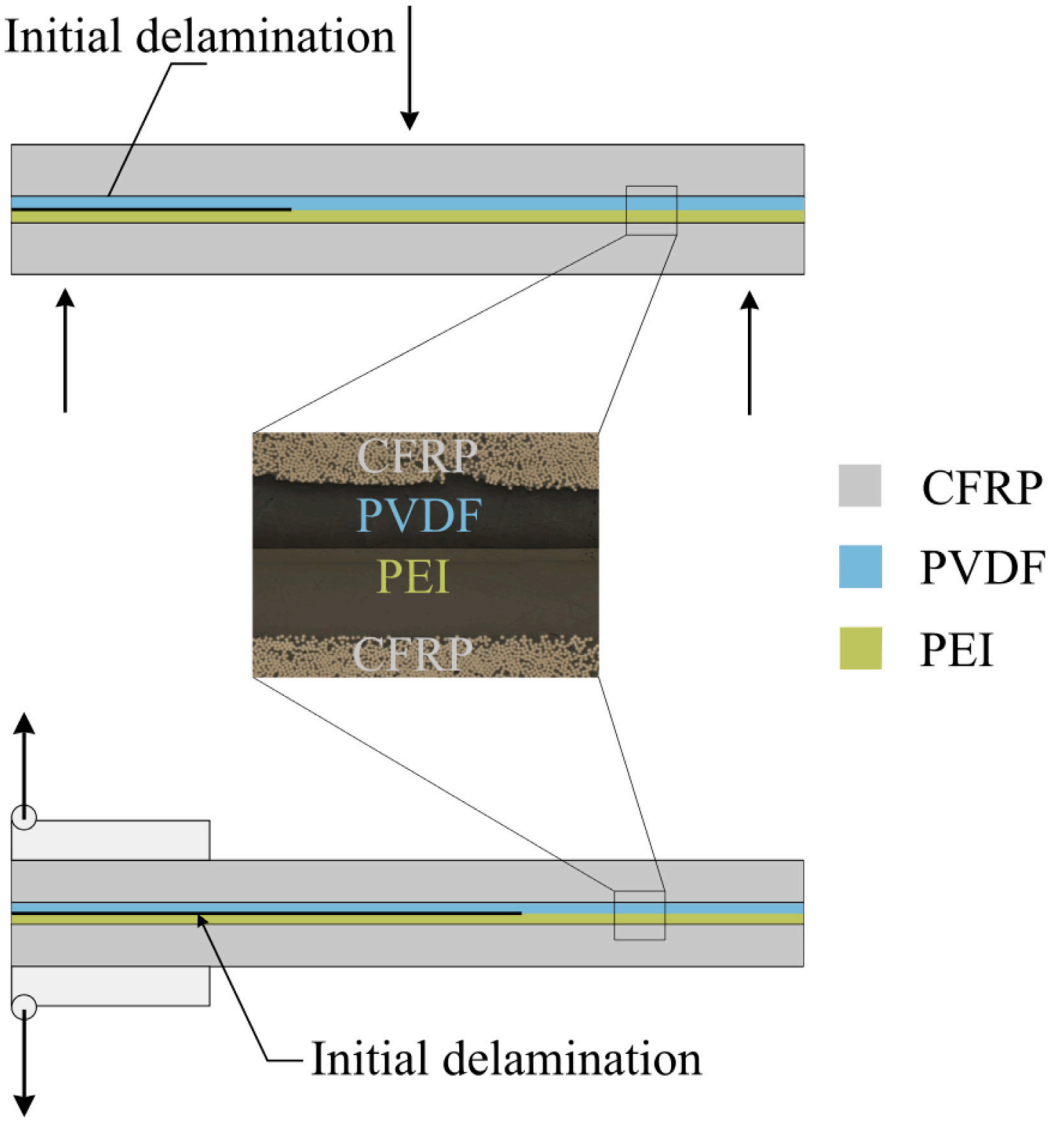

Fig. 2. ENF and DCB specimen configuration with PEI–PVDF Interface depicted with microscopy cross-section.

2.3. Specimen manufacturing

The DCB and ENF specimens (Fig. 2) are manufactured according to the geometry recommended in ASTM D5528 and ASTM D7905 (Tables 2, 3). The specimens were about 3 mm thick, which corresponds to 24 prepreg plies. This was the base configuration to test the CFRP–CFRP interface. The initial crack was realized by introducing a 12 µm thick ethylene-tetrafluoroethylene release (ETFE) film between the 12th and 13th prepreg ply. The initial crack length a_0 was 62 mm for the DCB specimens and 40 mm for the ENF specimens.

For the other configurations with extra material, one or two additional layers were placed between the 12th and 13th prepreg ply. For all configurations with one extra layer (PEI, PVDF and Adhesive), the release film is between the extra material and the adjacent prepreg ply. For the PEI–PVDF interface with two extra layers, the release film is placed directly on the PEI–PVDF interface instead. Fig. 2 shows the layup of the specimens for testing the PEI–PVDF interface, and Tables 2 and 3 indicate the ply-thickness of the additional layers for all configurations.

Each plate was cured in an autoclave. The specimens were cut from the manufactured plate, and piano hinges (25 mm × 25 mm × 1 mm) were bonded onto the DCB specimens with the room-curing Loctite EA 9466 epoxy adhesive after sanding the laminate and piano hinge surface to enhance the mechanical adhesion. Based on the study of Kyriazis [22], the piano hinges were bonded in reverse compared to the test standard. This measure reduces the possibility of premature failure of the bonded piano hinge.

Table 2
Parameter values for the DCB specimen.

Parameter	Value	Unit
Length, l_{DCB}	250.0	mm
Width, w_{DCB}	25.0	mm
Total thickness, t_t	3.26	mm
PEI–PVDF thickness, $t_{PEI--PVDF}$	0.15	mm
PEI thickness, t_{PEI}	0.025	mm
PVDF thickness, t_{PVDF}	0.1	mm
Initial crack length, a_0	62	mm

2.4. Mechanical testing and data reduction methods

DCB and ENF tests were performed on a Zwick/Roell Zwickiline universal testing machine equipped with a 5 kN load cell.

DCB tests were used to determine the cERR for Mode I. The energy release rate can be derived according to the fundamentals of Griffith's

Table 3
Parameter values for the ENF specimen.

Parameter	Value	Unit
Length, l_{ENF}	130.0	mm
Spanlength, L	100.0	mm
Width, w_{ENF}	25.0	mm
Total thickness, t_t	3.26	mm
PEI–PVDF thickness, $t_{PEI--PVDF}$	0.15	mm
PEI thickness, t_{PEI}	0.025	mm
PVDF thickness, t_{PVDF}	0.1	mm
Initial crack length, a_0	40	mm

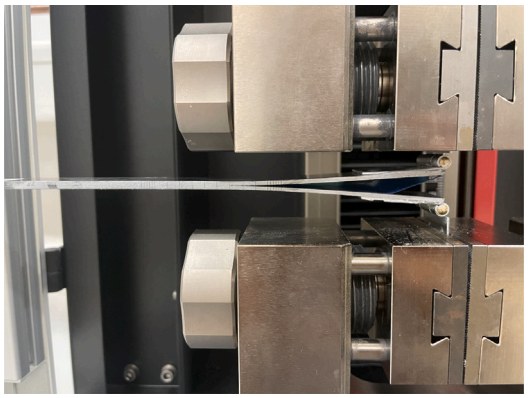

Fig. 3. DCB specimen inside fixture of testing machine according to ASTM D5528.

linear elastic fracture mechanics by simultaneously measuring load P, displacement d, and crack length a. The piano hinges of the specimen were mounted inside the clamping of the testing machine (see Fig. 3). First, the testing machine is operating with a testing speed of 2 mm/min to achieve a natural pre-crack as the starting condition of 3 to 5 mm. After unloading the specimen, the testing machine was driven at a constant crosshead speed of 1 mm/min for the test itself until a final crack length of 55 mm was observed. Crack length was measured during the test with a moving digital microscope. The applied load and the displacement were recorded and synchronized with crack length. For all specimens with PEI–PVDF interfaces and PVDF showing excessive, unstable crack growth, no natural pre-crack was introduced prior to testing, as initial precracking attempts resulted in unstable crack propagation, rendering the precracking step impractical for these configurations. The value of G_{Ic} was calculated using the Modified Beam Theory (MBT) method (Eq. (1)), as it is more conservative than the Compliance Calibration (CC) and Modified Compliance Calibration (MCCM) methods:

$$G_{Ic} = \frac{3Pd}{2w\left(a_0 + |\Delta|\right)} \tag{1}$$

where w is the width of the specimen and $|\Delta|$ is a correction accounting for imperfections compared to linear theory caused by rotations that may occur at the crack tip. The correction value $|\Delta|$ is experimentally determined by plotting the least squares of the cube root of compliance $C^{\frac{1}{3}}$ as a function of crack length. It should be noted that the correction does not include potential contributions from a process zone or fiber bridging.

ENF tests were conducted according to ASTM D7900 with the non-pre-cracked (NPC) method using a three-point bending fixture. The ENF specimens were placed on two supports with a diameter of d_1 = 5 mm and a distance of L = 100 mm (Fig. 4). The load is introduced by a central stamp with a diameter d_2 = 5 mm. This radius prevents from local damage due to indentation. A constant crosshead speed was set to 1 mm/min. Crack length is defined by the distance from the closest support to the inserted release film tip. Applied markings on

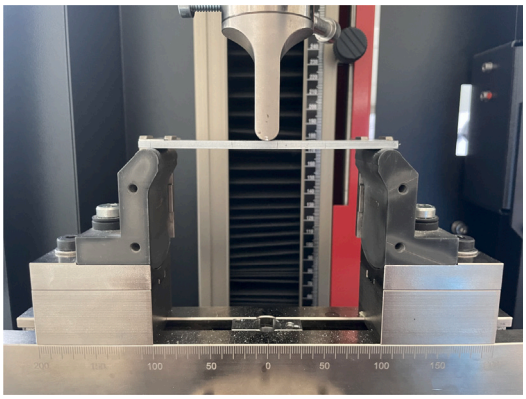

Fig. 4. ENF specimen inside 3-point-bend setup according to ASTM D7905.

the specimen facilitated the position of the specimen on the three-point bending fixture. As crack propagation is always unstable in ENF tests, crack propagation is not monitored.

The flexural modulus and the cERR of Mode II were obtained by the following Eqs. (2)–(4).

$$E_f = \frac{2L^3 + 3a_0^3}{8wt_t^3C} \tag{2}$$

$$G_{IIc} = \frac{9Pa_0^2d}{13w^2E_ft_t^3} \tag{3}$$

$$G_{IIc} = \frac{9Pa_0^2d}{2w(2L^3 + 3a_0^3)} \tag{4}$$

where the load P and the bending displacement d are taken at the occurrence of the crack, and w is the width of the specimen. The ASTM D7905 standard proposes non-pre-cracked (NPC) and pre-cracked (PC) test methods serving different purposes. In the NPC method, the specimen is loaded without the artificial pre-crack until the first significant load drop is observed. The specimen is then unloaded and the crack length after testing is measured. This advanced crack tip displays the initial crack length for the PC method. The difference between both methods reveals a more conservative cERR from the PC method, whereas the NPC method is faster to prepare since pre-cracking is not mandatory. Each method consists of a compliance calibration and fracturing step. So, one of each series is used to identify correction parameters for the compliance calibration (CC) method recommended in the test standard. Compliance C is determined by loading the specimen with 25 % of the critical loads at multiple simulated crack lengths by moving the specimen.

2.5. Microscopic methods

A Helios G4 CX (FEI) scanning electron microscope (SEM) equipped with energy dispersive X-ray spectroscopy (EDX) was used to study the fracture surfaces. Element mapping was conducted to analyze the chemical composition along the fracture surface. This should provide information about the crack path.

3. Experimental results and discussion

3.1. DCB test result

Fig. 5 shows the force–displacement curves from the DCB tests. For simplification, the PEI-, PVDF-, adhesive-, and CFRP–CFRP interfaces are denoted as PEI, PVDF, adhesive, and CFRP, respectively, in the following.

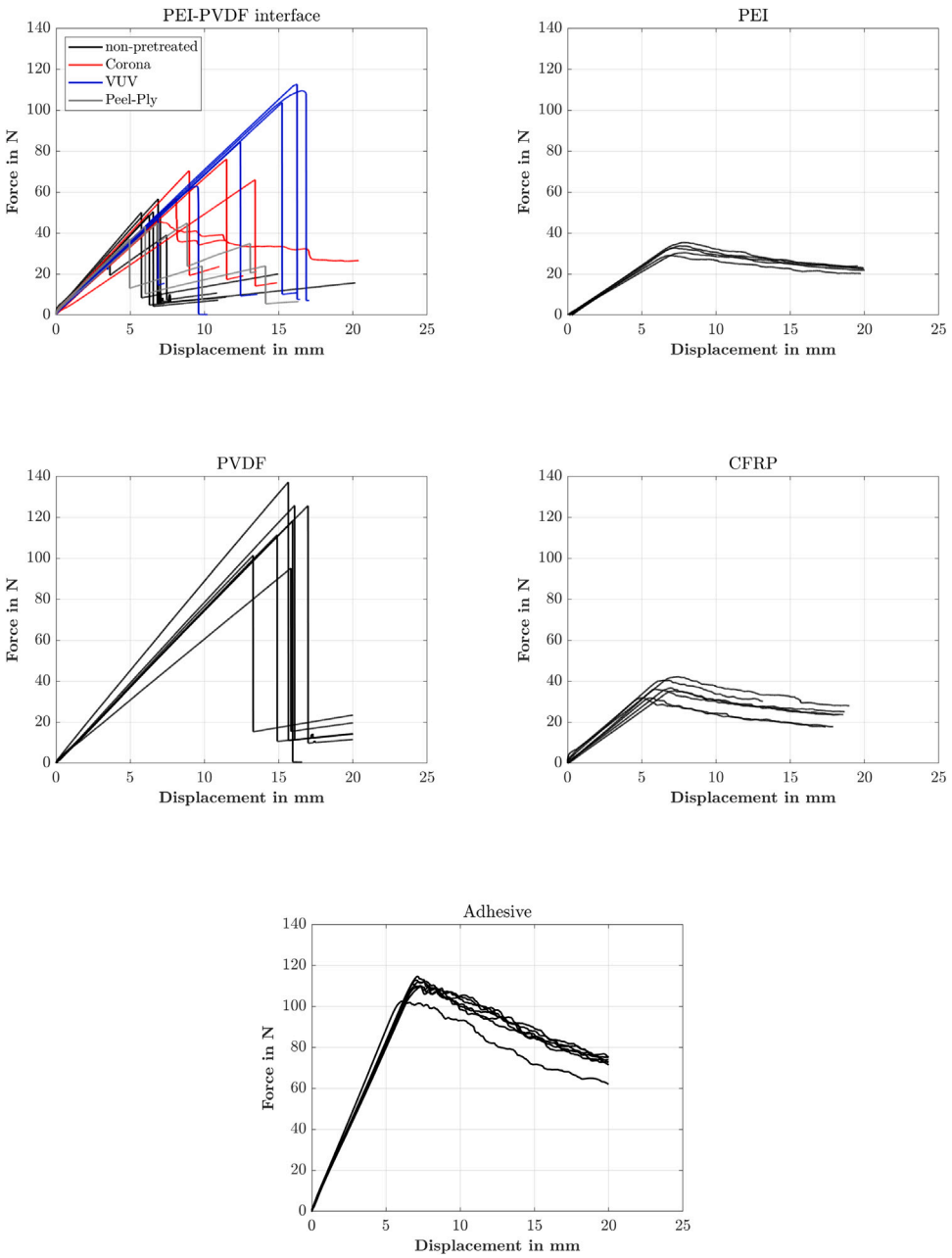

Fig. 5. Force–displacement curves of DCB tests of different interfaces.

All load–displacement data show linear behavior until the first load drop. Regarding the PEI–PVDF interface, it can be derived that the Peel Ply method decreased the damage load, while Corona pretreatment improves the damage initiation load up to 79 N. The damage initiation load of the specimens pretreated with VUV shows a higher scatter but a load up to 110 N. After damage initiation, an unstable crack propagation is observed for all PEI–PVDF interfaces and PVDF specimens, except for one Corona-pretreated specimen. In contrast to a stable crack propagation, where the force gradually decreases while the displacement increases, as seen for PEI, CFRP and film adhesive specimens, a discontinuous crack propagation appears as a distinct decrease in force between repeating crack growth and arrest. This behavior is known as "stick–slip", "non-smooth", or "crack plane mitigation" effect. An example of this stick–slip behavior of a Corona prepared specimen is shown in more detail in Fig. 6. With a sudden load drop (slip), the crosshead displacement does not change, but the crack propagation length changes fast. The fast crack propagation is arrested at a point followed by linear load increase at a lower stiffness (stick). The load decreases after one slip for the PEI–PVDF interfaces and PVDF by 90 %. The load drops for PEI, CFRP, and film adhesive specimens gradually in a stable manner throughout the propagation of the crack. The maximum load drop in this case is 40 %. The stick–slip behavior is related to the field of fracture dynamics. Due to the high propagation velocity of the crack during the slip phase (Fig. 6), the elastic strain energy is not entirely/directly converted into crack surface energy. Instead, part of the released energy is transformed into kinetic energy (causing a quick movement of the cantilever beams) and dissipated energy (such as plastic deformation at the crack tip).

This localized plastic deformation at the crack tip is particularly relevant for the PEI–PVDF interface and PVDF specimens, as PVDF is a semi-crystalline thermoplastic capable of plastic deformation. In contrast, for the CFRP and film adhesive specimens, which exhibit brittle fracture behavior, plastic dissipation at the crack tip is considered negligible. For PEI specimens, some limited viscoelastic or

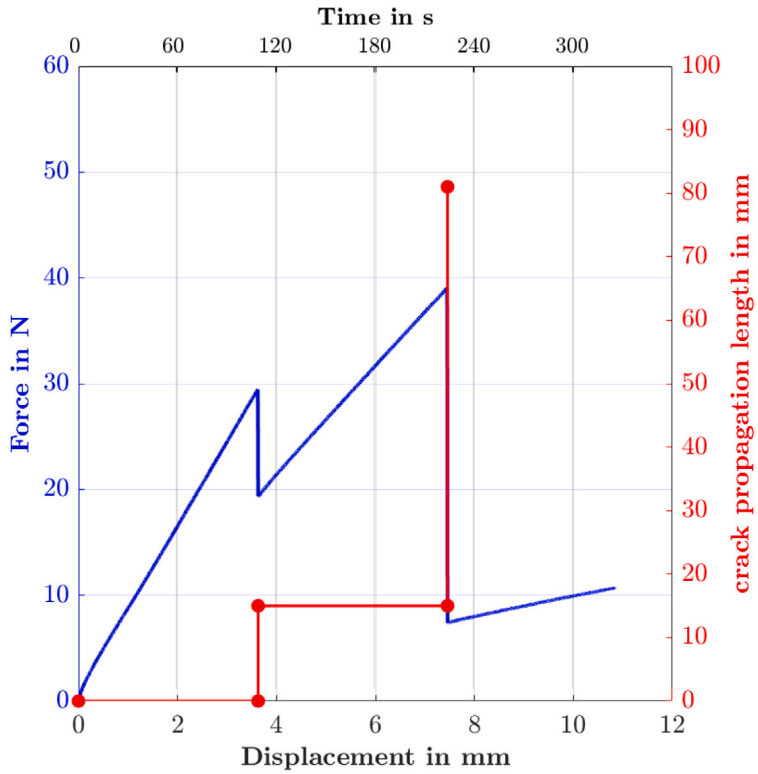

Fig. 6. Exemplary stick–slip behavior of one non-pretreated PEI–PVDF specimen: Load and crack propagation length over displacement and time.

plastic contribution cannot be excluded, but the observed stable crack propagation suggests that energy dissipation through plasticity remains minor compared to the crack surface energy.

In contrast to the stable case, where crack propagation occurs under quasi-static conditions, energy is transformed into crack surface energy with negligible kinetic energy [34].

The data for the R-curves are shown in Fig. 7, depicting G_{Ic} as a function of the crack length. This allows characterization of the initiation and propagation of the cracks. Specimens with PEI–PVDF interfaces and PVDF film show only two measurements of G_{Ic} due to a single distinct load drop. It can be found that there is a big difference between the initiation and arrest values. The R-curves of PEI–PVDF interfaces show the lowest G_{Ic} values for crack initiation for the Peel Ply method and the highest for the VUV pretreated specimens. However, the G_{Ic} values for the crack propagation decrease to almost 0 N/mm. The typical R-curve-effect, characterized by an increase in energy release rate with increasing crack length, is only observed for the monolithic CFRP in this study and is caused by fiber bridging, which is only observed for the monolithic CFRP in this study. Fiber bridging effectively increases the compliance of the specimen without a corresponding increase in crack length, such that neglecting it would lead to an overestimation of G_{Ic} and an artificially steep R-curve. However, since $|\Delta|$ as defined in ASTM D5528 accounts only for beam root rotation. Fiber bridging is thus not corrected. Several studies in the literature describe the influence of fiber bridging on the measured G_{Ic} value and propose corresponding correction terms or modified data reduction [35,36]. For all the other specimens, no fiber bridging was observed, and the correction $|\Delta|$ is therefore attributed solely to beam root rotation as described in Section 2.4.

While stable crack propagation has been extensively investigated, the literature considering unstable crack propagation is still limited. Kusaka et al. [37] proposed a rate-dependent dynamic crack growth model based on the energy balance principle, describing this instantaneous decrease in G_{Ic}. According to Kusaka et al. [37], the crack growth behavior of unidirectional CFRP could change from unstable to stable by increasing the loading-rate from 0.01 to 5 mm/min as inertia slows down the crack propagation velocity. Based on the Kusaka model, Zhou et al. [34] introduce a energy release rate ratio γ (Eq. (5))

$$\gamma = \frac{G_{Ic}^{init}}{G_{Ic}^{arr}} = \frac{(a_0 + \Delta a)^4}{a_0^4} \tag{5}$$

as an important parameter, being able to describe the degree of instability of a crack propagation. A higher value for γ leads to a larger difference between initiation cERR G_{Ic}^{init} and arrest cERR G_{Ic}^{arr}, a longer fast crack propagation phase, as well as a higher kinetic energy level. When γ is close to one, the initiation cERR is almost equal to the arrest cERR, which describes the stable propagation situation. In this study, the unstable crack growth specimens have a γ of up to 21, while the stable crack growth specimens show a γ of up to 1.5. This variable γ in the Kusaka model modified by Zhou et al. helps to describe the degree of instability, but does not fully explain why instable crack growth is observed for the considered interfaces. Webb et al. [38] stated that stick–slip crack growth is often observed in constant extension rate tests of viscoelastic polymers. The strain energy release rate is not only a function of the crack length but also depends on the crack tip velocity, where rate-dependent fracture processes occur. The rate-dependent viscoelastic behavior leads to stick–slip effects because the polymer cannot dissipate enough energy fast enough. This accumulated energy promotes sudden and quick crack jumps. From Hund et al. [39] and Pan et al. [40] it can be concluded that PVDF and PEI show a strongly rate-dependent deformation, explaining the tendency towards unstable crack growth observed in this study. However, the pristine PEI film shows stable crack propagation, which can be explained by discussing the G_{Ic} values below.

Fig. 8 presents the G_{Ic} of the PEI–PVDF interfaces with different surface pretreatments, the pristine films, monolithic CFRP, and film adhesive. A significant increase of 80 % for G_{Ic} can be achieved with VUV treatment. While no significant increase is measured using the Corona and the Peel Ply methods, Wang et al. [41] found that Peel Ply structured CFRP surfaces in a secondary adhesive bonding process

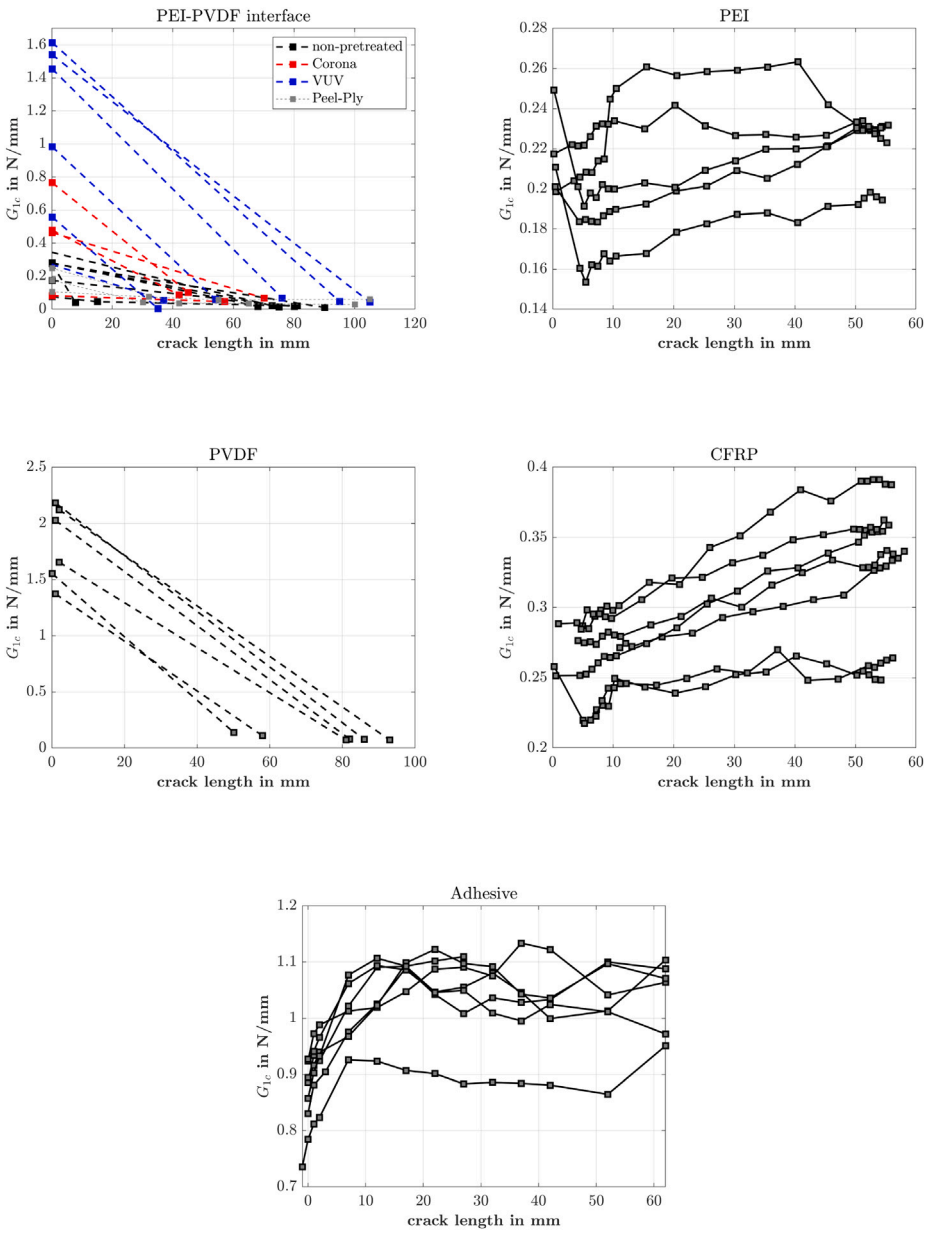

Fig. 7. R-curves of different pretreatment methods and pristine PEI, PVDF, CFRP and film adhesive in the DCB tests. Every line shows the R-curve of one specimen. The dashed lines guide the eye to highlight that no linear relationship is suggested between energy release rate and crack length.

do not increase the cERR in Mode I. They explain this tendency mainly with an unchanged contact angle between the Peel Ply structured and reference surface. However, Bérnard et al. [30] showed that a Peel Ply pretreatment increased surface energy by 40 %. In this study, the mechanical adhesion due to mechanical interlocking and the specific adhesion according to Kanerva et al. [42] based on an increase in surface polarity due to the use of polyamide Peel Ply do not come into play to a sufficient extent with the PEI–PVDF interface under consideration here. In contrast, specific adhesion appears to be improved by VUV and Corona treatment. There are limited insights about the influence of both surface pretreatment methods, compared with each other, on cERR. Oosterom et al. [43] showed no significant impact on shear strength for Corona- and VUV-pretreated PMMA substrates for different process parameters.

The non-pretreated PEI–PVDF interface is not weaker than CFRP, but weaker than the adhesive. The energy release rate in Mode I of the non-pretreated interface is 60 % smaller than the film adhesive's value. This confirms the observations that the failure of the multifunctional bondline in the CLS specimens occurs at this interface (Section 1). PVDF shows the highest G_{Ic} value with 1.84 N/mm. Löbel [26] reported for a PVDF film from the supplier Nowofol an energy release rate at 2.32 N/mm. The pristine PEI film shows almost the same G_{Ic} value as the monolithic CFRP. This finding contradicts the literature, since Bruckbauer [21] and Kyriazis [22] determined an increase of 50 % in G_{Ic} compared to the monolithic CFRP while observing a cohesive failure of the PEI. In this study, the specimens with the pristine PEI film show a fiber tear failure of the CFRP, which explains the G_{Ic} close to the CFRP value. The VUV treatment of the PEI–PVDF interface also leads to a significant increase from 0.22 to 1.2 N/mm which is in the standard deviation of the pristine PVDF and above that of the film adhesive.

Fig. 9 shows an image of the fracture surfaces of the DCB specimens with VUV-pretreated PEI–PVDF interfaces. Fig. 10 shows the fracture surface of the non-pretreated PEI–PVDF interface. On the right side, the area of the release film for the initial pre-crack is evident. Both specimen configurations apparently show adhesive failure between the PEI–PVDF interface. However, the pretreated and non-pretreated

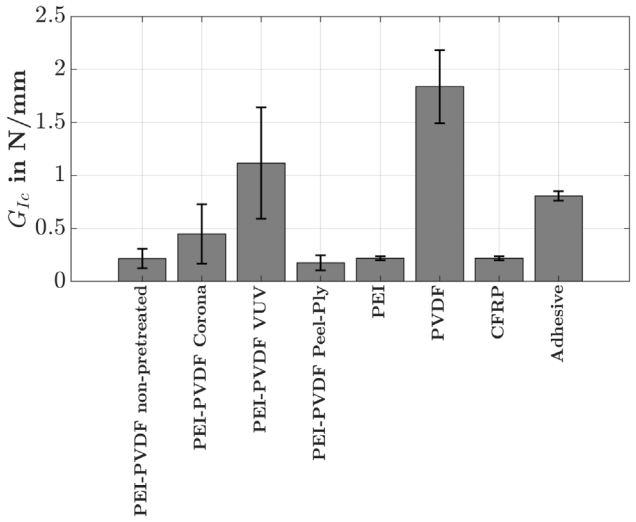

Fig. 8. Influence of VUV-, Corona and Peel Ply PEI–PVDF treatment methods compared to pristine PEI, PVDF, CFRP and film Adhesive on Mode I cERR.

specimens show differences in energy release rate and their fracture surfaces. The PEI and PVDF films appear mat, whereas the fracture surfaces of the non-pretreated specimen show a barely unchanged appearance compared to the initial state before integration. The stick–slip behavior mentioned above in Fig. 6 can also be observed on the fracture surface of the VUV pretreated specimen (Fig. 9). The area of each propagated crack displays quasi-parabolic crack front curves. This suggests that the crack length determined at the edges of the specimens during the test differs from the maximum crack length in the middle of the specimens. Considering this, the true energy release rates should be slightly lower than the calculated value. The PEI and PVDF films show a stress whitening phenomenon (crazing) at each crack initiation stage in Fig. 9. This results from the plastic flow and crazing processes of the films [39]. Crazing forms a process zone ahead of the crack tip, dissipating energy. Since the correction $|\Delta|$ as defined in the ASTM D5528 addresses only beam root rotation and elastic deformation, the energy dissipated within the process zone is not corrected. Consequently, the determined G_{Ic} values for VUV pretreated PEI–PVDF interface are likely overestimated, as the dissipated energy from crazing and plasticity is attributed to the crack surface energy formation. Differences in the fracture surfaces and the average G_{Ic} indicate different adhesion mechanisms.

Fig. 11 shows the results of SEM analysis with EDX mapping of the crack surfaces depicted in Figs. 10 and 9. The overall distribution of the elements and the corresponding spectrum are depicted. The half specimen with PEI surface without surface preparation shows oxygen

Table 4
Position of crack and distinction between cohesive (CF), adhesive (AF), special-cohesive (sCF) and fiber-tear-failure (FTF)for the DCB specimen configuration.

Specimen config.	Crack length a in mm	Failure type
PEI–PVDF untreated	130–152	AF
PEI–PVDF Corona	107–197	AF
PEI–PVDF VUV	99–167	sCF
PEI–PVDF Peel Ply	93–104	AF
PEI	114–117	FTF
PVDF	105–148	CF
CFRP	109–111	CF
Adhesive	168–172	CF

sulfite (Fig. 11a), whereas with VUV pretreatment, a significant amount of fluoride is detected at the same level as oxygen (Fig. 11c). The specimen halves with PVDF surfaces (Fig. 11b,d) are unchanged in terms of element types.

Although the failure mode appears adhesive on a macroscopic level (Fig. 9) in the VUV-pretreated samples, the detection of fluoride on the PEI fracture surface indicates that the crack did not propagate strictly along the PEI–PVDF interface. Instead, the presence of fluoride on the PEI side suggests a partial cohesive failure within the PVDF layer, consistent with a special cohesive failure according to DIN EN ISO 10365. This implies that VUV pretreatment promotes intermolecular interaction at the PEI–PVDF interface, resulting in a failure mode that is adhesive in appearance but cohesive in nature at the microscopic level, contributing to the specific adhesion. Table 4 summarizes the failure types and the crack lengths.

3.2. ENF test result

Fig. 12 shows the recorded load–displacement curves for the ENF tests. The specimens with the VUV-, Corona-pretreated, and non-pretreated PEI–PVDF interface show failure at force levels of 1754 to 2329 N. The displacement at crack initiation is between 8 and 12 mm. The failure load of specimens with Peel Ply structured PEI in the interface is significantly lower with a minimum crack initiation load at 700 N. CFRP, film adhesive, and PEI specimens show similar maximum deformation, while PVDF and PEI–PVDF specimens have higher deformation up to 13 mm.

The calculated G_{IIc} values from the load–displacement curves are depicted in Fig. 13. The non-pretreated PEI–PVDF interface shows a mean G_{IIc} of 12.4 ± 3.4 N/mm. Corona and VUV pretreatment improve the mean G_{IIc} value up to 14.1 and 13.5 N/mm respectively, yet the error bars for the standard deviation overlap. It should be mentioned that the standard deviation of the G_{IIc} values of Corona pretreated specimens is at least 2.4 N/mm lower compared to the non-pretreated and VUV specimens. The Peel Ply approach significantly decreases the energy release rate under Mode II to 4.6 N/mm. This indicates

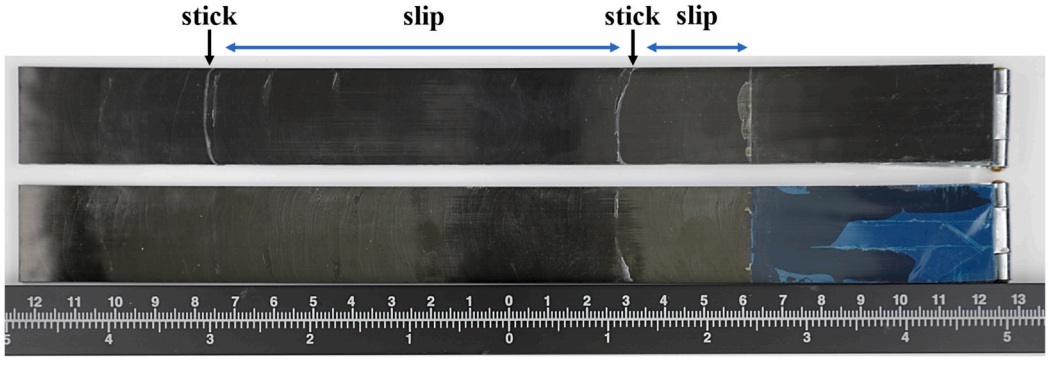

Fig. 9. Crack surface of VUV pretreated DCB specimen.

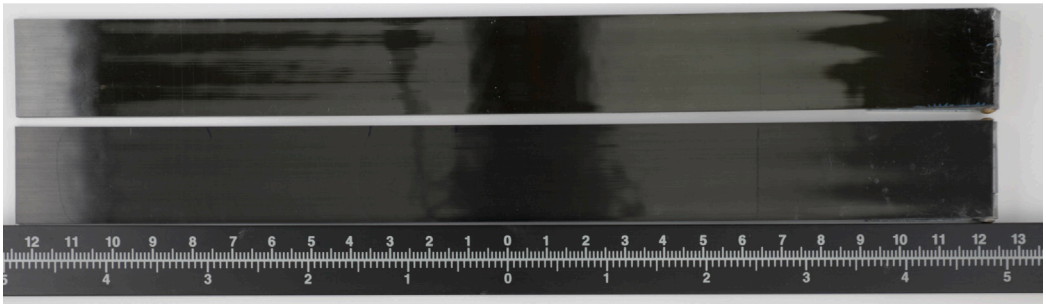

Fig. 10. Crack surface of non-pretreated DCB specimen.

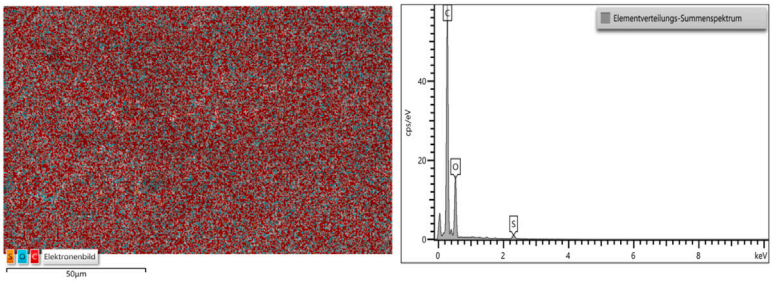

(a) specimen half with PEI surface non-pretreated

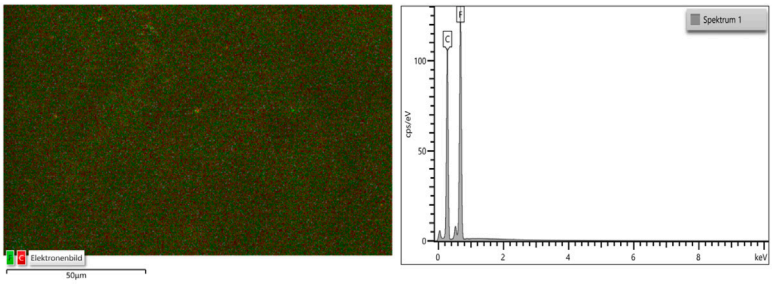

(b) specimen half with PVDF surface non-pretreated

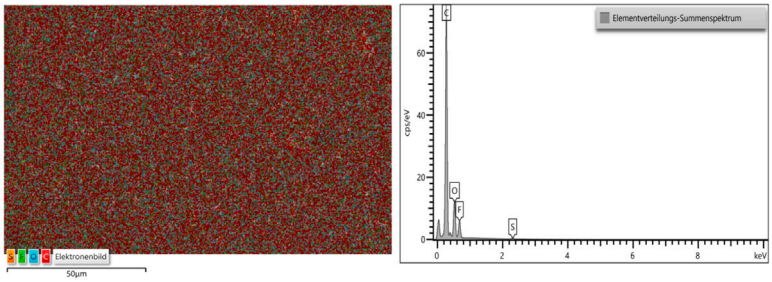

(c) specimen half with PEI surface with VUV pretreatment

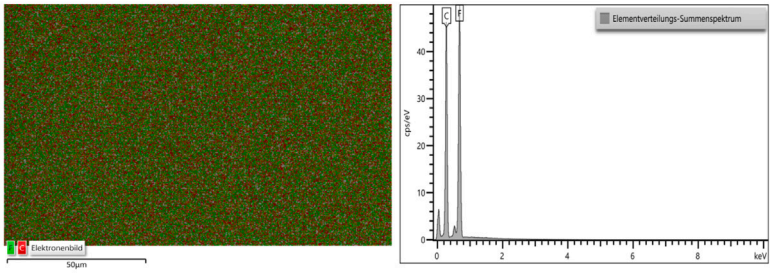

(d) specimen half with PVDF surface with VUV pretreatment

Fig. 11. EDX surface analysis - right: element spectrum, left: element distribution.

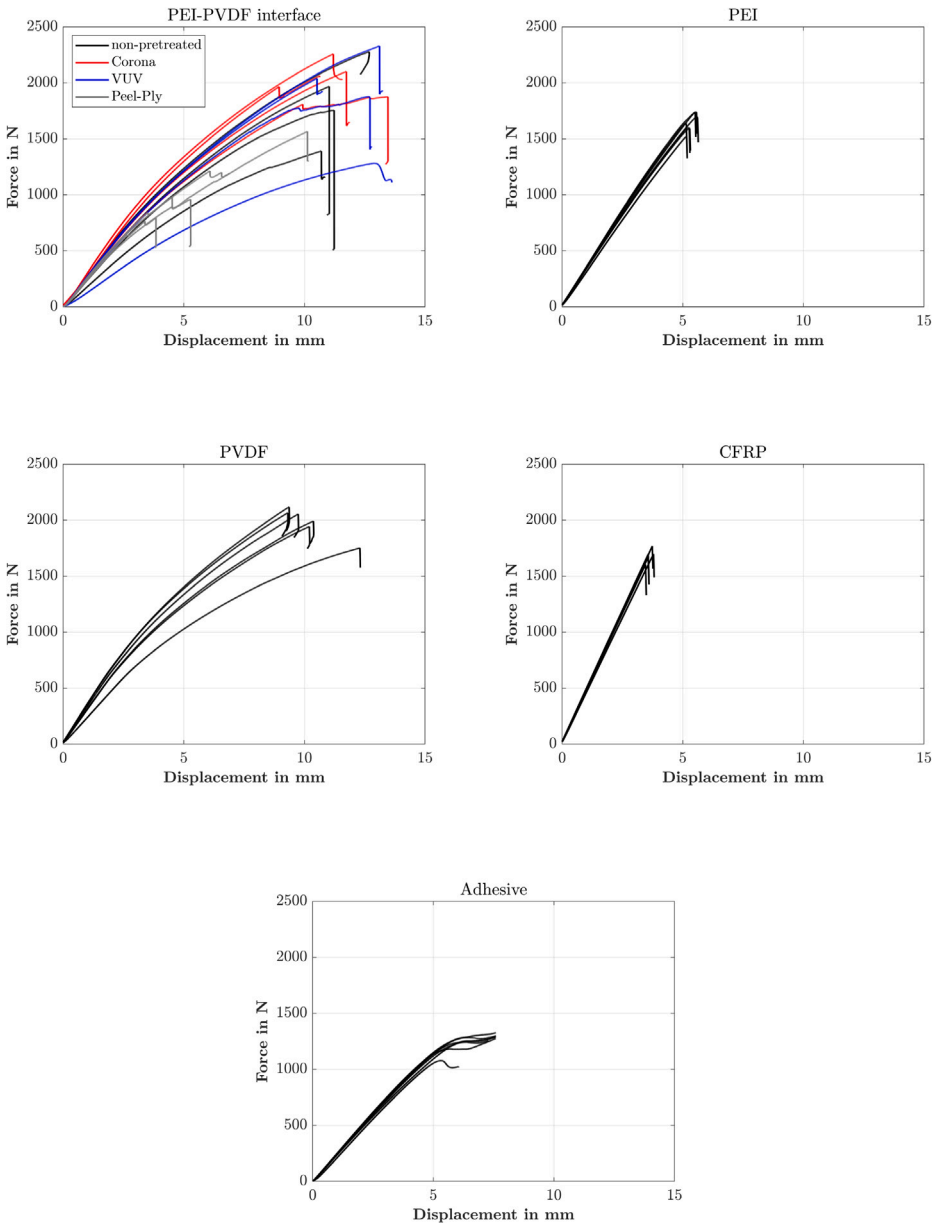

Fig. 12. Force–displacement curves of ENF tests of different interfaces of ENF tests.

that the VUV and Corona methods perform at a comparable level in terms of failure load and mean G_{IIc} value. No substantial advantage is observed for any of the specific pretreatments, except for the decreased deviation and thus higher reproducibility for the Corona pretreatment. The pristine 0.025 mm thick PEI film shows an energy release rate at the level of the 0.150 mm thick PEI–PVDF Peel Ply prepared specimen. There is no significant improvement towards the monolithic CFRP. The pristine PVDF film increases the G_{IIc} value compared to the CFRP and film adhesive, however, the value does not differ significantly from the PEI–PVDF interface. Thus, the investigated PEI–PVDF interfaces as well as the pristine films do not weaken the CFRP and the film adhesive under Mode II.

Compared to the G_{Ic} value, the mean G_{IIc} value of the non-pretreated PEI is lower than that of the non-pretreated PEI–PVDF interface. This could be explained by the influence of the interface thickness on the energy release rate observed under Mode II. A thicker interface (PEI–PVDF) tends to a higher cERR [44]. This effect is weaker for Mode I load case in DCB specimens [45,46]. Another comparison between the different pretreated PEI–PVDF interfaces proves that the cERR in Mode I is more sensitive to adhesion mechanisms than in Mode II.

Since the G_{IIc} value of the non-pretreated PEI–PVDF interface is higher than that of the film adhesive, Mode I may be, despite the lower amount in the MMR of the CLS specimen, the more critical case for MDAF as the primary cause of adhesive failure between PEI and PVDF. Through enhancement of the interfacial adhesion between PEI and PVDF by VUV treatment, it can be ensured that the MDAF is not the weakest link in the multifunctional bondline. This hypothesis is based on the significantly increased G_{Ic} values. Future CLS tests with VUV-pretreated PEI–PVDF interfaces would be required to experimentally confirm whether the improved interfacial fracture toughness is sufficient to prevent early adhesive failure under the combined Mode I and Mode II loading conditions present in the CLS configuration.

4. Conclusions

This study investigated the weak adhesion between PEI and PVDF. In previous implementations, this interface proved to be the weakest

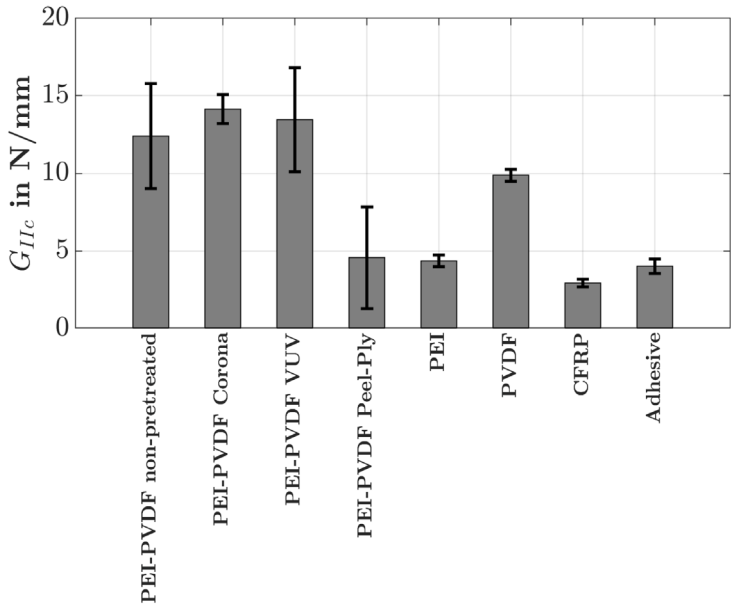

Fig. 13. Influence of VUV-, Corona and Peel Ply PEI–PVDF treatment methods compared to pristine PEI, PVDF, CFRP and Adhesive on Mode II cERR.

link in a multifunctional bondline adding strain monitoring and a disbond arrest feature to the adhesive bond, showing early adhesive failure. The Mode I and Mode II loads acting on the bondline in a CLS specimen form the background of the present investigation based on DCB and ENF tests with VUV-, Corona, and Peel Ply-pretreated PEI–PVDF interfaces. The G_{IIc} values do not change significantly with the chosen surface treatment. However, the G_{IIc} of the interface is higher than that of the film adhesive. The G_{Ic} values for the non-pretreated PEI–PVDF interface are lower than those of the film adhesive and can be significantly increased by VUV treatment to be in the range of the disbond-arresting PVDF. This suggests that the Mode II case contributes less to the observed adhesion failure between PEI and PVDF in the CLS specimen. The significantly lower G_{Ic} value of the non-pretreated interface may be more likely to contribute to the failure. The fact that the G_{Ic} value can be increased by VUV treatment may prevent an early failure at the interface between the PEI sensor inlay and the PVDF disbond arrest in CLS specimens. Future CLS tests with improved interfaces could prove that the MDAF is not the weakest link in the multifunctional bondline, preventing the structural bond from early failure.

The insights gained in this paper regarding the improvement of the adhesion of the PEI–PVDF interface can significantly enhance the robustness of the sensor system itself, enabling the detection and localization of crack growth through mechanical strain measurement.

CRediT authorship contribution statement

Riem Kilian: Writing – review & editing, Writing – original draft, Visualization, Software, Methodology, Investigation, Data curation, Conceptualization. **Ann-Kathrin Klein:** Writing – review & editing, Resources, Conceptualization. **Julian Steinmetz:** Writing – review & editing, Resources, Conceptualization. **Martin Johannes Schollerer:** Writing – review & editing, Resources, Conceptualization. **Christian Hühne:** Writing – review & editing, Supervision, Project administration, Funding acquisition. **Andreas Dietzel:** Writing – review & editing, Supervision, Project administration, Conceptualization. **Oliver Völkerink:** Writing – review & editing, Supervision, Project administration, Funding acquisition, Conceptualization.

Declaration of competing interest

The authors declare that they have no known competing financial interests or personal relationships that could have appeared to influence the work reported in this paper.

Acknowledgments

This research was funded by the Deutsche Forschungsgemeinschaft (DFG, German Research Foundation) - 401136681.

Data availability

The raw and processed data required to reproduce the above findings are available to download from https://doi.org/10.5281/zenodo.15781418.

References

[1] Hart-Smith LJ. Adhesively bonded joints in aircraft structures. In: da Silva LFM, Öchsner A, Adams RD, editors. Handbook of adhesion technology. Cham: Springer International Publishing; 2018, p. 1235–84. http://dx.doi.org/10.1007/978-3-319-55411-2_44.

[2] Habenicht G. Kleben: Grundlagen, technologien, anwendungen. Berlin, Heidelberg: Springer; 2009, http://dx.doi.org/10.1007/978-3-540-85266-7.

[3] Schmid Fuertes TA, Kruse T, Körwien T, Geistbeck M. Bonding of CFRP primary aerospace structures – Discussion of the certification boundary conditions and related technology fields addressing the needs for development. Compos Interfaces 2015;22(8):795–808. http://dx.doi.org/10.1080/09276440.2015.1077048.

[4] Waite S. 19 - Certification and airworthiness of polymer composite aircraft. In: Irving P, Soutis C, editors. Polymer composites in the aerospace industry. Woodhead publishing series in composites science and engineering, second ed.. Woodhead Publishing; 2020, p. 593–645. http://dx.doi.org/10.1016/B978-0-08-102679-3.00019-8.

[5] European Union Aviation Safety Agency. Annex II to ED decision 2010/003/R of 19/07/2010. 2022, Available online: https://www.easa.europa.eu/sites/default/files/dfu/Annex%20II%20-%20AMC%2020-29.pdf. [Accessed 25 May 2020].

[6] Federal Aviation Administration. Advisory circular 20-107B – Composite aircraft structure. 2010, Available online: https://www.faa.gov/documentLibrary/media/Advisory_Circular/AC_20-107B.pdf. [Accessed 1 January 2010].

[7] Adams RD, Drinkwater BW. Nondestructive testing of Adhesively-Bonded joints. NDT E Int 1997;30(2):93–8. http://dx.doi.org/10.1016/S0963-8695(96)00050-3.

[8] Sachse R, Pickett A, Middendorf P. Analysis of crack-arrest design features for adhesively bonded composite joints: An experimental and numerical study. Compos Struct 2021;274:114301. http://dx.doi.org/10.1016/j.compstruct.2021.114301.

[9] Chowdhury N, Chiu WK, Wang J, Chang P. Static and fatigue testing of thin riveted, bonded and hybrid carbon fiber double lap joints used in aircraft structures. Compos Struct 2015;121:315–23. http://dx.doi.org/10.1016/j.compstruct.2014.11.004.
[10] Steinmetz JBS. Functional compliance of multifunctional bondlines with disbond arrest and health monitoring features for safe and efficient composite joints (Ph.D. thesis), 2024.
[11] Schollerer M. Steigerung der robustheit von strukturellen verklebungen in der luftfahrt mittels lokaler oberflächenzähmodifikation (Ph.D. thesis), 2024, http://dx.doi.org/10.57676/5fb5-dr68, ISSN: 1434-8454 Publisher: Technische Universität Braunschweig.
[12] Schollerer M, Kosmann J, Völkerink O, Holzhüter D, Hühne C. Surface toughening – a concept to decrease stress peaks in bonded joints. J Adhes 2019;95(5–7):495–514. http://dx.doi.org/10.1080/00218464.2018.1555041.
[13] Völkerink O, Hühne C. Virtual testing for design and certification of (fusion) bonded longitudinal joints in a fibre composite fuselage: A proposal using FEM-based progressive damage analysis. Compos C 2022;7:100236.
[14] von der Heide C. Integrable sensors on foil for smart systems and bondline surveillance (Ph.D. thesis), DE: Shaker Verlag GmbH; 2024, http://dx.doi.org/10.2370/VdHeide2024.FoilSensors, [Accessed 11 December 2024].
[15] Heide Cvd, Steinmetz J, Völkerink O, Makiela P, Hühne C, Sinapius M, Dietzel A. Polyetherimide-Reinforced smart inlays for bondline surveillance in composites. Polymers 2022;14(18):3816. http://dx.doi.org/10.3390/polym14183816, Number: 18 Publisher: MDPI AG.
[16] Tsai SW. Double–Double: New family of composite laminates. AIAA J 2021;59:1–11. http://dx.doi.org/10.2514/1.J060659.
[17] Farooq U, Sakarinen E, Teuwen J, Alderliesten R, Dransfeld C. Synergistic toughening of epoxy through layered poly(ether imide) with dual-scale morphologies. ACS Appl Mater Interfaces 2023;15(45):53074–85. http://dx.doi.org/10.1021/acsami.3c10096, Publisher: American Chemical Society.
[18] Quan D, Farooq U, Zhao G, Dransfeld C, Alderliesten R. Co-cured carbon fibre/epoxy composite joints by advanced thermoplastic films with excellent structural integrity and thermal resistance. Int J Adhes Adhes 2022;118:103247. http://dx.doi.org/10.1016/j.ijadhadh.2022.103247.
[19] Lestriez B, Chapel J-P, Gérard J-F. Gradient interphase between reactive epoxy and glassy thermoplastic from dissolution process, reaction kinetics, and phase separation thermodynamics. Macromolecules 2001;34(5):1204–13. http://dx.doi.org/10.1021/ma0012189.
[20] Tsiangou E, Teixeira de Freitas S, Fernandez Villegas I, Benedictus R. Investigation on energy director-less ultrasonic welding of polyetherimide (PEI)-to epoxy-based composites. Compos B 2019;173:107014. http://dx.doi.org/10.1016/j.compositesb.2019.107014.
[21] Bruckbauer P. Struktur-eigenschafts-beziehungen von interphasen zwischen epoxidharz und thermoplastischen funktionsschichten für faserverbundwerkstoffe (Ph.D. thesis), Technische Universität München; 2018, URL https://mediatum.ub.tum.de/1427427.
[22] Kyriazis A. Bauteilintegrierte überwachung variothermer faserverbundfertigungsprozesse mittels minimalinvasiver foliensensoren auf löslichem substrat. Mechanics and adaptronics, Berlin, Heidelberg: Springer Berlin Heidelberg; 2024, http://dx.doi.org/10.1007/978-3-662-68165-7.
[23] Laurien M, Demir B, Büttemeyer H, Herrmann AS, Walsh TR, Ciacchi LC. Atomistic modeling of the formation of a thermoset/thermoplastic interphase during Co-Curing. Macromolecules 2018;51(11):3983–93. http://dx.doi.org/10.1021/acs.macromol.8b00736, Publisher: American Chemical Society.
[24] Arikan ES. Oberflächenmodifikation von polyetheretherketon (PEEK) für das strukturelle kleben in der luftfahrt (Ph.D. thesis), München: Universität der Bundeswehr München; 2020, ISBN: 978-3-8439-4584-4 Series: Luftfahrt.
[25] Johnson WS. Stress analysis of the cracked lap shear specimens: An ASTM round robin. Tech. rep. NAS 1.15:89006, 1986, NTRS Author Affiliations: NASA Langley Research Center NTRS Document ID: 19860021599 NTRS Research Center: Legacy CDMS (CDMS).
[26] Löbel T. The hybrid bondline: a novel disbond-stopping design for adhesively bonded composite joints (Ph.D. thesis), 2016.
[27] Wang C. Introduction to fracture mechanics. 1996, http://dx.doi.org/10.13140/RG.2.1.1444.2408, Available via ResearchGate.
[28] Völkerink O. Simulation-driven design of bonded joints in fibre composite aircraft structures using progressive damage analyses (Ph.D. thesis), 2022, http://dx.doi.org/10.57676/hya4-2a09, ISSN: 1434-8454 Num Pages: 308 Publisher: Technische Universität Carolo-Wilhelmina zu Braunschweig.
[29] Hexcel. HexPly 8552 epoxy matrix product data. 2012.
[30] Ourahmoune R, Salvia M, Mathia T, Berthel B, Fouvry S, Mesrati N. Effect of sandblasting substrate treatment on single lap shear strength of adhesively bonded PEEK and its composites. 2011, Journal Abbreviation: ICCM International Conferences on Composite Materials Publication Title: ICCM International Conferences on Composite Materials.
[31] Arikan E, Holtmannspötter J, Zimmer F, Hofmann T, Gudladt H-J. The role of chemical surface modification for structural adhesive bonding on polymers - Washability of chemical functionalization without reducing adhesion. Int J Adhes Adhes 2019;95:102409. http://dx.doi.org/10.1016/j.ijadhadh.2019.102409.
[32] Arikan E, Holtmannspötter J, Hofmann T, Gudladt H-J. Vacuum-UV of polyetheretherketone (PEEK) as a surface pre-treatment for structural adhesive bonding. J Adhes 2020;96(10):917–44. http://dx.doi.org/10.1080/00218464.2018.1545646, Publisher: Taylor & Francis _eprint: https://doi.org/10.1080/00218464.2018.1545646.
[33] Klein A-K, Kilian R, Von der Heide C, Steinmetz J, Hühne C, Völkerink O, Dietzel A. Screen-printed polyetherimide smart inlays for surveillance of bonded joints in composite structures. Compos C 2025. submitted for publication.
[34] Zhou Y, Xiao Y, Wu Q, Xue Y. A multi-state progressive cohesive law for the prediction of unstable propagation and arrest of Mode-I delamination cracks in composite laminates. Eng Fract Mech 2021;248:107684. http://dx.doi.org/10.1016/j.engfracmech.2021.107684.
[35] Sørensen BF, Jacobsen TK. Large-scale bridging in composites: R-curves and bridging laws. Compos A 1998;29(11):1443–51. http://dx.doi.org/10.1016/S1359-835X(98)00025-6.
[36] Gur HB, Banks-Sills L. Evaluation of the effect of fiber bridging on mode I quasi-static testing. Fatigue Fract Eng Mater Struct 2023;46(4):1357–74. http://dx.doi.org/10.1111/ffe.13930.
[37] Kusaka T, Hojo M, Mai Y-W, Kurokawa T, Nojima T, Ochiai S. Rate dependence of mode I fracture behaviour in carbon-fibre/epoxy composite laminates. Compos Sci Technol 1998;58(3–4):591–602. http://dx.doi.org/10.1016/S0266-3538(97)00176-0.
[38] Webb TW, Aifantis EC. Crack growth resistance curves and stick-slip fracture instabilities. Mech Res Commun 1997;24(2):123–30. http://dx.doi.org/10.1016/S0093-6413(97)00003-7.
[39] Hund J, Granum HM, Olufsen SN, Holmström PH, Johnsen J, Clausen AH. Impact of stress triaxiality, strain rate, and temperature on the mechanical response and morphology of PVDF. Polym Test 2022;114:107717. http://dx.doi.org/10.1016/j.polymertesting.2022.107717.
[40] Pan D-x, Kang G-z, Zhu Z-w, Liu Y-j. Experimental study on uniaxial time-dependent ratcheting of a polyetherimide polymer. J Zhejiang Univ-Sci A 2010;11(10):804–10. http://dx.doi.org/10.1631/jzus.A1000131.
[41] Wang D, Li Y, Zou T, Fu J, Liu Z. Increasing strength and fracture toughness of carbon fibre-reinforced plastic adhesively bonded joints by combining peel-ply and oxygen plasma treatments. Appl Surf Sci 2023;612:155768. http://dx.doi.org/10.1016/j.apsusc.2022.155768.
[42] Kanerva M, Saarela O. The peel ply surface treatment for adhesive bonding of composites: A review. Int J Adhes Adhes 2013;43:60–9. http://dx.doi.org/10.1016/j.ijadhadh.2013.01.014.
[43] Oosterom R, Ahmed TJ, Poulis JA, Bersee HEN. Adhesion performance of UHMWPE after different surface modification techniques. Med Eng Phys 2006;28(4):323–30. http://dx.doi.org/10.1016/j.medengphy.2005.07.009.
[44] Ji G, Ouyang Z, Li G. Effects of bondline thickness on mode-II interfacial laws of bonded laminated composite plate. Int J Fract 2011;168(2):197–207. http://dx.doi.org/10.1007/s10704-010-9571-9.
[45] De Freitas ST, Budzik MK. Bondline thickness: Fracture mechanics perspective. In: Advances in structural adhesive bonding. Elsevier; 2023, p. 615–41. http://dx.doi.org/10.1016/B978-0-323-91214-3.00027-2.
[46] Lee D-B, Ikeda T, Miyazaki N, Choi N-S. Effect of bond thickness on the fracture toughness of adhesive joints. J Eng Mater Technol 2004;126(1):14–8. http://dx.doi.org/10.1115/1.1631433.